Journal of Electroanalytical Chemistry 862 (2020) 114016

Contents lists available at ScienceDirect

Journal of Electroanalytical Chemistry

journal homepage: www.elsevier.com/locate/jelechem

Electrochemical performance of thin free-standing boron-doped diamond nanosheet electrodes

Robert Bogdanowicz [a,*], Mateusz Ficek [a], Natalia Malinowska [b], Sanju Gupta [c], Romney Meek [c], Paweł Niedziałkowski [b], Michał Rycewicz [a], Mirosław Sawczak [d], Jacek Ryl [e], Tadeusz Ossowski [b]

[a] Department of Metrology and Optoelectronics, Faculty of Electronics, Telecommunications and Informatics, Gdańsk University of Technology, 11/12 Narutowicza St., 80-233 Gdańsk, Poland
[b] Department of Analytical Chemistry, Faculty of Chemistry, University of Gdańsk, 63 Wita Stwosza St., 80-308 Gdańsk, (Poland)
[c] Department of Physics and Astronomy, Western Kentucky University, Bowling Green, KY 42101, USA
[d] Centre for Plasma and Laser Engineering, The Szewalski Institute of Fluid-Flow Machinery, Polish Academy of Sciences, 14 Fiszera St., 80-231 Gdańsk, (Poland)
[e] Department of Electrochemistry, Corrosion and Material Engineering, Faculty of Chemistry, Gdańsk University of Technology, 11/12 Narutowicza St., 80-233 Gdańsk, (Poland)

ARTICLE INFO

Article history:
Received 17 July 2019
Received in revised form 18 December 2019
Accepted 26 February 2020
Available online 27 February 2020

Keywords:
Boron-doped diamond
Free-standing diamond nanosheets
Cyclic voltammetry
Electron transfer mechanism

ABSTRACT

In the following work we describe preparation and the electrochemical performance of thin and free-standing heavy boron-doped diamond (BDD) nanosheets. The investigated foils were deposited on Ta substrate using microwave plasma-enhanced chemical vapor deposition technique (MPECVD). Foils of two B-dopant densities were investigated, obtained on the base of 10 k and 20 k ppm [B]/[C] ratio in the gas admixture. The obtained foils can be easily peeled from substrate in deionized water to be then attached to other material, in this case polydimethylsiloxane (PDMS). We have shown that the top surface and the bottom side of investigated boron-doped diamond nanosheet possess significantly altered morphology and physico-chemical properties, revealed by electron microscopy, Raman spectroscopy and electrochemistry. The voltammetric response of investigated BDD foils as working electrodes indicates the highest activity for the nanosheet with higher dopant concentration, in particular on its top surface. Furthermore, electrodes are characterized with altered kinetics, characteristic for partially blocked electrodes with quasi-reversible charge transfer.

1. Introduction

The BDD (boron-doped diamond) electrodes are of great interest, especially in the field of diverse electronic [1] and electrochemical devices [2], including transistors [3], biosensors [4], energy converters [5] and energy harvesters [6]. The remarkable electrochemical properties of BDD film makes it a very promising material for the third-generation biosensors [7] combining sensitivity and specificity with the advantages of novel microelectronics. BDD modified electrodes also provide fast electrochemical response in comparison to glassy carbon [8]. However, a number of new applications are limited by the high temperature of the CVD growth of diamond. To overcome this problem, we propose utilizing free-standing nanocrystalline diamond (NCD) foils and thin diamond nanosheets on polymer substrates. Here, we consider that the thin diamond material could be transferred to other substrates by the standard scotch-tape techniques employed in 2D materials and multi-layered electronic devices. In addition, free-standing undoped non-conductive diamond films could be applied as a dielectric barrier or their boron-doped counterparts, as a semiconducting p-type layer or a biosensing surface.

The boron doped diamond provides other unique properties that make it an ultra-sensitive electroanalytical platform for electrochemical sensing [9–11], biosensing [12,13], and electrocatalysis [14–16]. As an electrode material, diamond provides a wide electrochemical potential window from -1.25 *V* to $+2.3$ V SHE (standard hydrogen electrode) in aqueous electrolytes [17,18], as well as high anodic stability [19], chemical inertness, [20,21] and biocompatibility. [22,23]

Besides the electrochemical performance, the high transparency of thin CVD diamond films over the whole region from the ultraviolet to the far-infrared spectral region allows for novel technological applications to optical coatings, [24,25] optoelectronic switching devices, [26] or high-speed near-infrared photodetectors. [27] A few attempts to fabricate the diamond foil have been reported in the literature. Seshan et al. [28] demonstrated a versatile transfer technique based on an all-dry viscoelastic stamping to pick up NCD films grown by CVD that were later thinned by wet and plasma etching. Next, Lodes et al. [29] and Fecher et al. [30] reported stripped-off hot-filament CVD grown diamond foils by using a Nd:YAG laser.

Electrochemical analytical techniques are powerful methods that can easily provide many information about novel materials and their electrochemical properties [31]. The unmodified BDD electrodes are widely used to determination of different analytes [32]. Yang et al. [33] showed wide overview of the electrical and electrochemical properties revealing

* Corresponding author.
E-mail address: rbogdan@eti.pg.edu.pl. (R. Bogdanowicz).

http://dx.doi.org/10.1016/j.jelechem.2020.114016

its importance. Recent research areas range from in-vivo bioelectrochemistry and neuronal/retinal stimulation advanced oxidation processes [34], supercapacitors [35] to the extended electroanalysis of organic compounds, biomolecules [36] and pharmaceuticals [37]. Recently, Diaz et al. [38] manifested that BDD enables production of a powerful oxidant that could be used for water treatment purposes without generating toxic by-products. This group reported that direct electron transfer from the BDD and an indirect oxidation through •OH radicals is driving the generation of ferrate. Next, Ivandini et al. [39] performed first-principles molecular dynamics simulations and electrochemical studied at various BDD crystal orientations and surface terminations showing that polycrystalline BDD is the most reactive, whereas the (111) samples proved to be more reactive than the (100) ones for single-crystal BDD.

In the present paper, we describe the electrochemical properties of both sides of thin diamond foils/nanosheets that could be used as freestanding electrodes. We demonstrate electrochemical behavior of a reference redox system by using voltammetric techniques with thin boron-doped diamond nanosheets transferred to polymer substrate as working electrodes. Potassium ferrocyanide was employed for evaluating the electrochemical properties of thin diamond nanosheet electrode. To date, there is no report of fabricating high-area thin diamond nanosheets transferred to flexible polymer substrate along with detailed electrochemical investigation.

2. Experimental

2.1. Free-standing boron-doped diamond nanosheets

The growth of boron-doped diamond nanosheets was carried out in microwave plasma enhanced chemical vapor deposition (MPECVD; 2.45 GHz Seki Astex 6400) system using CH_4(1%)/H_2 plasma with microwave power of 1300 W, pressure 50 Torr and substrate temperature 500 °C. The doping level was set to 10 k and 20 k ppm [B]/[C] consuming diborane precursor during the growth process (attn. 1% and 2% of B in plasma). The films were deposited at the mirror polished Ta ⟨100⟩ substrates and detail deposition procedure is given in our earlier report [40,41]. The undoped nanodiamond seeds were used during Ta pre-treatment. The density of seeding was limited to minimize the contribution of the undoped seeds to the interfacial resistance as reported by group of Hantschel et al. [42].

The growth time was set to 180 min and 100 min for 10 k and 20 k ppm [B]/[C] nanosheets respectively, producing films of comparable thickness of ca. 350 nm.

Subsequently, the boron-doped diamond foils were self-peeled off from Ta substrate and floated over the surface of DI water [43]. The process and sides of diamond foil were illustrated in Fig. 1. Next, the diamond foil was fish out by polydimethylsiloxane (PDMS) sheet to fabricate nanosheet-polymer sample with approx. diamond diameter of 5 mm. The resistivity of samples was measured on the both sides of diamond nanosheets at room temperature by a four-point probe with an interprobe spacing of s = 1.6 mm and needle probes with a 10 μm diameter. The four-point probe was connected to the source meter (Keithley 2400, UK). Sheet resistivity was calculated according to the formula (1):

$$R_s\ (\Omega{\cdot}cm) = 4,532{\cdot}\frac{V}{I}{\cdot}t, \quad (1)$$

where t is thickness (cm), V is voltage measured at the internal probes, and I is the current applied to the external probes.

The Raman spectra of diamond foils were recorded using micro Raman spectrometer (InVia, Renishaw, UK) equipped with 514 nm Ar^+ laser as an excitation source and 100 × objective. Spectra were recorded in a range of 100–3200 cm^{-1} on the top side of diamond film (Top Surface) as well as on the reverse side of diamond layer delaminated from the metal substrate (Bottom Side).

The morphologies of free standing boron-doped diamond foils were inspected using scanning electron microscope FEI Quenta FEG 250 with 10 kV beam accelerating voltage and SE-ETD detector (secondary electron – Everhart-Thornley detector) working in high vacuum mode (pressure 0.1 mPa). We have analyzed the 2d areas of separated crystals using manual mode of outlining shapes in the SEM image. Analysis and visualization of the data was performed by Fiji software (Windows 64-bit portable version) [44].

2.2. Cyclic voltammetry setup

Electrochemical measurements were carried out on a potentiostat AutoLab PGStat 128 N (Metrohm) with conventional three-electrode configuration at room temperature. All potentials during experiments were measured versus the Ag/AgCl electrode. The PDMS with ultra-thin boron-doped diamond nanosheet was used as a working electrode and platinum wire as a counter electrode. The area of the working surface was ca. 0.2 cm^2 (disk diameter: 5.0 mm) and was not treated electrochemically before measurements. The direct contact was made to the electrode by pressing sheet of aluminum foil at the studied surface. Potassium ferrocyanide ($K_4Fe(CN)_6$) was chosen as a reference redox probe system at concentration 5 mM in 0.5 M Na_2SO_4. The optimized conditions for cyclic voltammetry: the potential ranging from ca. -0.3 to 0.8 V and scan rate 10–100 mV/s without resistance compensation. The boron-doped diamond nanosheets was also studied in solution containing $Ru(NH_3)_6^{3+/2+}$ used as outer redox species. All measurements were obtained in 5 mM of $Ru(NH_3)_6^{3+/2+}$ dissolved in 0.5 M Na_2SO_4 solution performing different scan rates from 10 V/s to 100 V/s.

3. Results and discussion

3.1. Morphology of boron-doped diamond nanosheet electrodes

Scanning electron microscopy is a great tool for analyzing the morphology of the crystallites. Even, at the early stage of the CVD, this method was used to study effect of temperature, pressure and level of doping on the size of the diamond. The photos of the top surface and bottom side of the diamond foils with different B/C ratio registered using SEM were presented in Fig. 2.

The nanocrystals from the bottom side are flat in contrast to the crystallites, which are present on the top surface. It is caused by the direct contact of the bottom side with the tantalum. The black spots presented in the microimages results from interfacial defects like amorphous or graphitic carbon forms grown during nucleation phase.

The effect of boron doping on the crystal area of the diamond was investigated. The results were listed in Table 1.

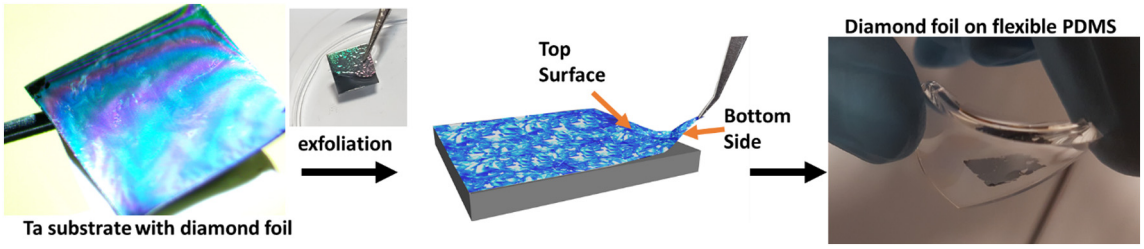

Fig. 1. Isolation and transfer of boron-doped diamond nanosheets to PDMS polymer substrates.

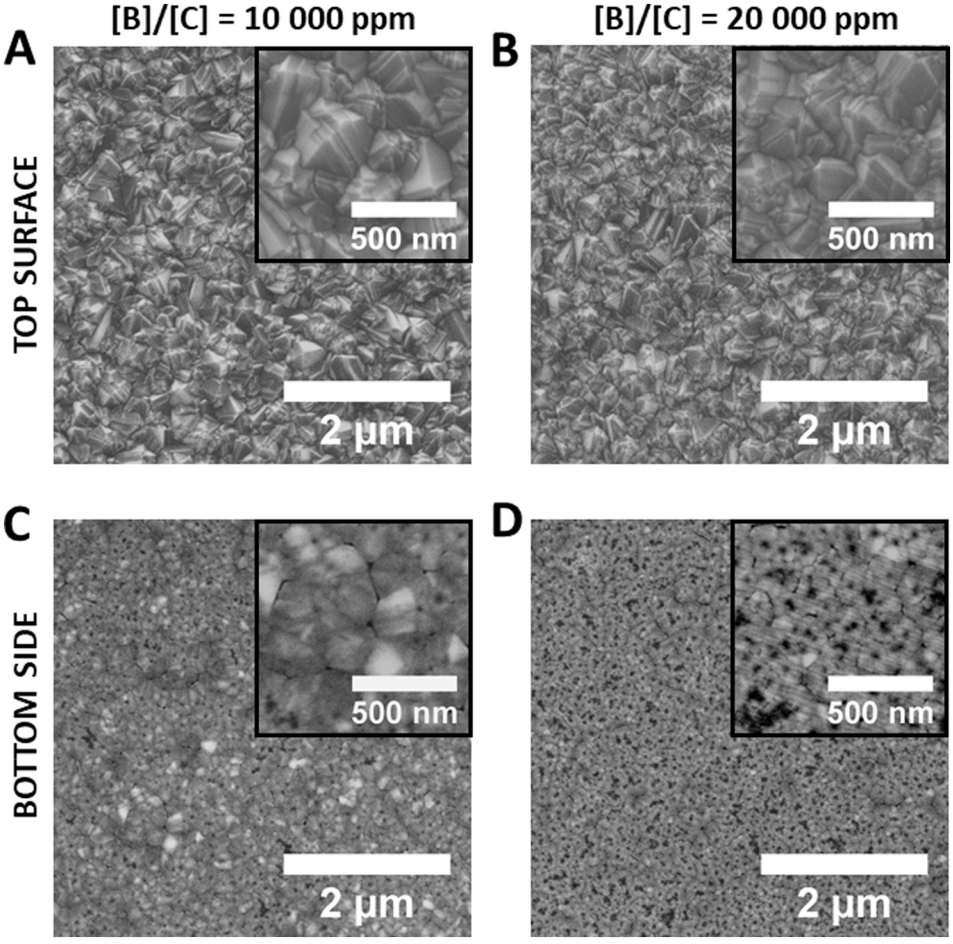

Fig. 2. The morphology of thin free – standing boron doped diamond nanosheets in the function of the boron doping: (A) [B]/[C] 10 k ppm, top surface; (B) [B]/[C] 20 k ppm, top surface; (C) [B]/[C] 10 k ppm, bottom side; (D) [B]/[C] 20 k ppm, bottom side.

Higher B/C ratio in the chamber during chemical vapor deposition process causes smaller grain area. Top surface sample with doping level 10 k has 25% crystallites, which area is >0.06 μm^2. For 20 k, top surface sample we achieved 20% grains, which size is higher than 0.06 μm^2. The differences between grain area of top surface and bottom side are caused that the backside has more non-diamond carbon phases and the boron incorporates into the diamond structure after certain time.

3.2. Molecular structure of BDD nanosheet investigated by Raman spectroscopy

Morphologic data are confirmed Raman spectroscopy (RS) that is an important nondestructive analytical tool to gather information about molecular and crystal lattice vibrations. It is used to characterize carbon-based materials since it is sensitive to different types of carbon–carbon bonding, polymorphism, and is capable of monitoring changes in Raman bands when the size of the crystals is decreased to nanoscale and for boron-doped diamond films. Fig. 3 shows the Raman spectra of two of the heavily boron-doped diamond nanosheet samples ([B]/[C] 10 k ppm, and [B]/[C] 20 k ppm) top and bottom sides. They both show characteristic first-order diamond (sp^3 C phase) band (D), which is redshifted by a few wavenumbers ~1291 cm^{-1}–1327 cm^{-1} (ca. 1332 cm^{-1} characteristic of single crystal diamond) *albeit* relatively broad Γ_{FWHM} = 11.4 cm^{-1} (ca. 1.1 cm^{-1}) and asymmetric with Fano line shape.

However, the shift in the diamond (D) peak is in the opposite direction to those assigned typically due to phonon confinement [45,46]. The wide asymmetric band with maximum near 500 cm^{-1} (B1) accompanied with smaller one near 1210 cm^{-1} (B2) originate from the boron defects and it's appearance can be observed for the boron doping level ≥10 k ppm. The band B2 overlap with the diamond band (D) centered in the range of wavenumbers form 1290 to 1327 cm^{-1} depending of the boron doping level. The intensity of band (B2) grows with respect to diamond band (D) that is indicative of substitution of boron for carbon atoms. Due to the Fano effect and shift of the Raman peaks caused by high boron doping the D band at 1350 cm^{-1} cannot be distinguished in 20 k sample. Additionally, the broad band ranged between 1450 and 1550 cm^{-1} assigned to non-diamond region and a mix of bending and stretching modes of various CC, CH, and CO containing surface functionalities.

As shown in Table 2 clear differences in band positions can be observed for samples with the B/C ratio at the level of 10 k ppm and 20 k ppm. As reported by other authors the position of B1, B2 and D bands move to the smaller wavenumbers with the increase of the boron doping level and the linear dependence of the of B/C ratio and band position can be observed

Table 1
Grain area of ultra – thin free – standing boron doped diamond nanosheets.

Grain area (GA) μm^2	[B]/[C] = 10,000 ppm		[B]/[C] = 20,000 ppm	
	Top	Bottom	Top	Bottom
GA < 0.02	12.5%	17.7%	16%	12.2%
0.02 < GA < 0.06	62.5%	76.4%	64%	78.8%
0.06 < GA < 0.1	19%	5.9%	16%	6%
0.1 < GA < 0.14	6%	0%	4%	3%

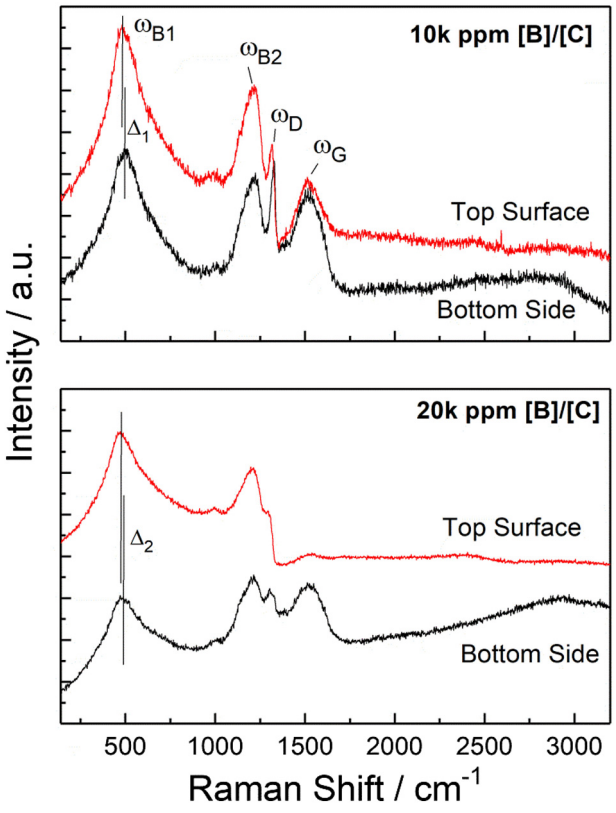

Fig. 3. Raman spectra recorded for top surface and bottom side of boron-doped diamond nanosheet samples: [B]/[C] 10 k ppm, and [B]/[C] 20 k ppm.

[47]. The use of relationship [47] between boron level measured by SIMS and B1 and B2 Raman band positions allows for estimation of boron dopant concentrations. The average boron concentration was $1.60{\cdot}10^{21}$ cm^{-3} and $2.67{\cdot}10^{21}$ cm^{-3} for 10 k ppm and 20 k ppm of top side of nanosheets respectively. It is worth noting that the boron concentration estimated at the bottom side of the film is lower and reaches $1{\cdot}10^{21}$ cm^{-3} and $2.06{\cdot}10^{21}$ cm^{-3} for 10 k ppm and 20 k ppm correspondingly. The difference in boron concentration observed for the same diamond nanosheet achieved at the top and bottom side is also confirmed by the SEM observation and is mainly attributed to the boron doping suppression in the first stage of diamond growth.

3.3. Cyclic voltammetry investigation: Redox mediator influence

The electrochemical performance of boron-doped diamond nanosheets transferred to PDMS, namely 10 k and 20 k was particularly studied. The surface resistivity of sample was first examined by means of 4-point probe. The resistivity of the top surface (10*k*) showed a value of 640 mΩ·cm, while the back side reached 2.46 Ω·cm. Correspondingly, the 20 k sample results in 43 mΩ·cm (top surface) and 26 mΩ·cm (bottom side). Results are summarized in Table 3.

Table 2
Position of ω (B1), ω (B2) and ω (B3) Raman bands assigned for top surface and bottom side of two membrane samples with [B]/[C] 10 k ppm, and [B]/[C] 20 k ppm.

Sample	ω (B1)/cm^{-1}	ω (B2)/cm^{-1}	ω (D)/cm^{-1}
10 k Bottom	503.2	1215	1327
10 k Top	495.3	1210	1315
20 k Bottom	487.6	1207	1303
20 k Top	479.3	1202	1291

Table 3
Electronic parameters of the diamond nanosheet.

Sample	Resistance (Ω)	Resistivity (mΩ·cm)
10 k Bottom	15.5 k	2460
10 k Top	4034	640
20 k Bottom	273	43
20 k Top	165	26

The differences in the conductivity of both surfaces reveals fact that the undoped seeds and boron suppression plays an important role during the initial stage of *CVD* growth. Since the top surface and the back side of these nanosheets present various structures and conductivity, as revealed by SEM micrographs and 4 point probe measurements, both of these surfaces were investigated electrochemically separately for comparison purposes.

Fig. S1 (Supplementary Information) shows the cyclic voltammograms of studied boron-doped diamond nanosheets obtained in 0.5 M Na_2SO_4 estimated from −1.5 to 1.5 V for bottom and top surface for 10 k and 20 k respectively. The range of potential windows recorded for top surfaces are significantly shorter than for the obtained for the bottom surfaces. The shape of cyclic voltammograms can suggest that 20 k boron-doped diamond nanosheets measured at top surface can contain some sp^2 impurities [48]. The capacitance of boron-doped diamond nanosheets were calculated according to the procedure described by Śmietana et al. [49] are listed in Table S1 (Supplementary Information). The capacitance for 20 k measured at bottom side is ca. 10 time higher than capacitance for 10 k boron-doped diamond nanosheets, measured at bottom side, while the value of capacitance was determined for 20 k boron-doped diamond nanosheets measured at top surface is almost 2.2 times higher than capacitance obtained for 10 k top sides.

Chronovoltammetry (CV) studies were carried out in 0.5 M Na_2SO_4 electrolyte containing 5 mM $K_4Fe(CN)_6$ redox couple, the polarization range was −0.3 to 0.8 V vs. Ag|AgCl. These measurements were repeated at different scan rates in the range of 10–500 mV/s (see Fig. 4). The $[Fe(CN)_6]^{-3/-4}$ was chosen as an efficient and main redox system to evaluate boron-doped diamond nanosheets electrochemical activity and characterize surface. Nevertheless, the preliminary EC studies in $Ru(NH_3)_6^{3+/2+}$ revealed peak-to-peak separations ΔE = 125 mV (see Fig. S2 in Supplementary Information) similar to typical reversible electrochemical processes, while the $[Fe(CN)_6]^{-3/-4}$ redox system results here in the significant variability in function of the scan rate.

The Faradaic reaction was observed for each investigated sample in the presence of the redox-active species and within determined potential window. The results at the top surface and bottom side of BDD nanosheet electrodes reveal significant differences in kinetics of the charge transfer process between various materials. These are a result of differences in structural properties of boron-doped diamond nanosheets. The electrochemical results are summarized in Table 4.

Among all tested materials, the lowest peak-to-peak separation value was found for the top surface of 20 k nanosheets and was equal to 73 mV at 10 mV/s scan rate. This value is only slightly higher than what is expected for a Nernstian one-electrode reaction and indicate the reversibility of the electrochemical process and low level of surface coverage by contamination species. The electrodes with lower dopant concentration did not show as high reversibility, regardless of analyzed nanosheet side. However, for electrochemically reversible processes, the half-peak potential $E_{p/2}$ of the forward scan should be 56.5 mV [51]. In our study it was slightly higher, but did not exceeded 70 mV for 20 k and 78 mV for 10 k nanosheets, respectively. It should be noted that the peak current ratio I_{red}/I_{ox} is similar to 1, what is also expected from reversible systems. To summarize, all the electrodes possess close-to-reversible, *quasi*-reversible character, while 20 k top side electrode is to highest extent diffusion controlled. Following results support the theory that that reaction plane of these electrodes reveal overall lower activity. There are multiple factors affecting the charge transfer kinetics of BDD electrodes: doping concentration [52], crystalline size

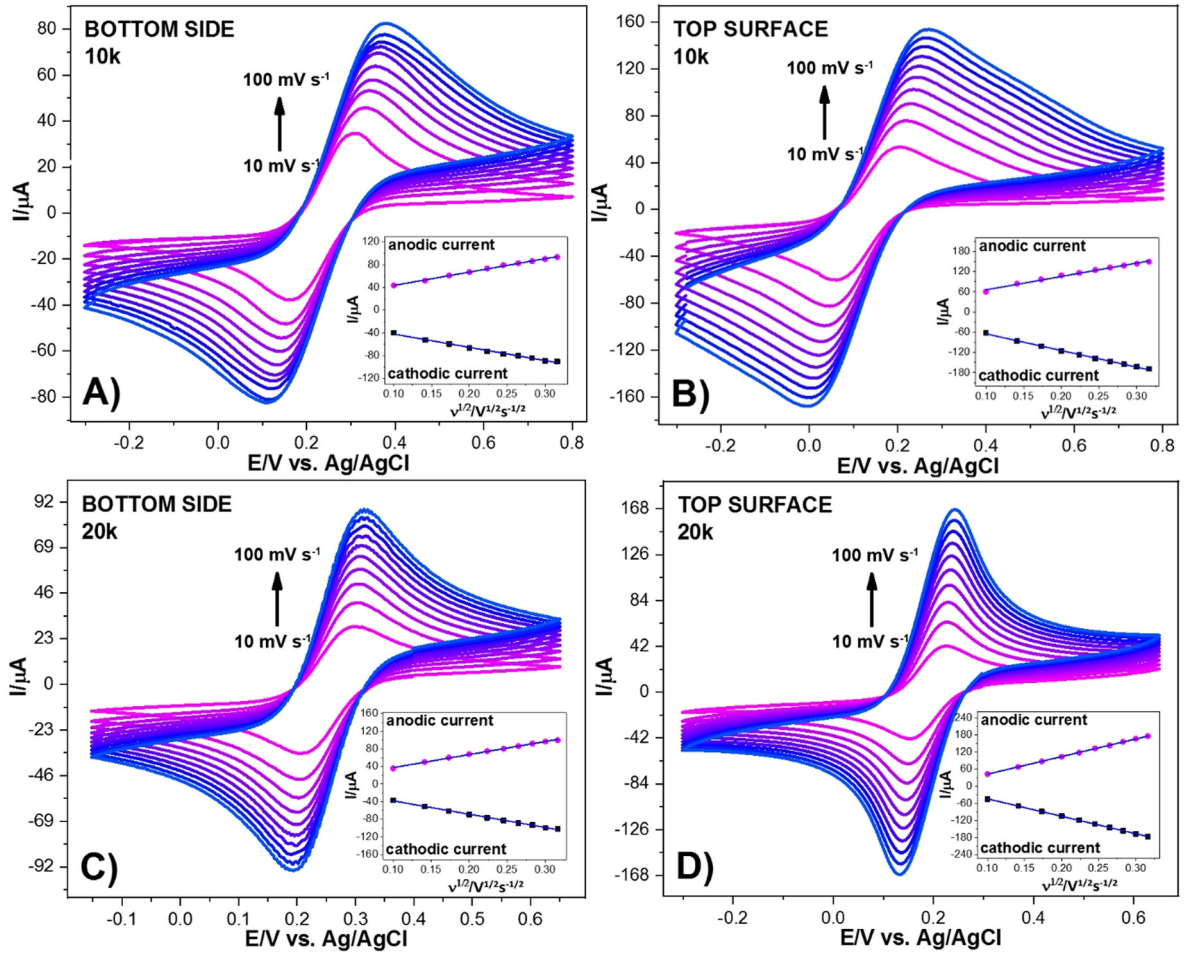

Fig. 4. Cyclic voltammograms of 5 mM $Fe(CN)_6^{3-/4-}$ redox system in 0.5 M Na_2SO_4 on the boron-doped diamond nanosheet electrodes at different scan rates in the range of 10–100 m*V*/s for (A) bottom side of 10 k, (B) top surface of 10 k, (C) bottom side of 20 k, (D) top surface of 20 k nanosheet. Insets: anodic and cathodic peak currents versus square root of scan rates.

due to uneven conductivity at grain boundaries [53], crystallographic orientation [54], type of termination [55,56] etc. The micron and submicron size of these features should result to heavily overlapping diffusion fields, while the broadening of the CV peaks, in particular for the bottom side of 10 k and 20 k electrodes might suggest existence of partially blocked electrode mechanics, limited by adsorbed contamination species [57,58]. The following hypothesis is confirmed with Raman results, showing surface functionalities assigned to non-diamond features in 1450–1550 cm^{-1} range.

Furthermore, CV peaks observable at the top surface of 10 k BDD nanosheet electrodes reveal anodic peak broadening, suggesting existence of a more complex electron charge transfer by $Fe(CN)_6^{4-}$ species. Similar behavior was not observed for 20 k samples.

Table 4
Summary of voltammetric data: formal redox potential E^f ($E^f = (E^{ox} + E^{red})/2$), peak potential separation ΔE, half-peak potential $E_{p/2}$ and standard reaction rate constant k_0. k_0 was estimated for investigated electrodes with approach proposed by Holze [50]. Electrolyte: 5 mM $K_4Fe(CN)_6$ in 0.5 M Na_2SO_4 solution, scan rate 10 mV/s.

Redox system	Doping	Side	E^f/mV	ΔE / mV	$E_{p/2}$/mV	$k_0/\times 10^{-1}$ cm/s
$Fe(CN)_6^{3-/4-}$	10 k	Top surface	143	144	78	0.246
		Bottom side	244	149	77	0.229
	20 k	Top surface	187	73	61	2.509
		Bottom side	254	98	70	1.571

Formal redox potential E^f for $Fe(CN)_6^{3-/4-}$ process, obtained for 20 k top surface nanosheet electrode was equal to +187 mV vs Ag|AgCl, while for all the remaining electrodes shown similar values, ranging from 244 to 265 mV. The possible explanation for different behavior between these electrodes is due to higher reversibility of 20 k top surface electrode, since the value of formal standard potential for quasi-reversible processes depends on equilibrium constant k^0 and symmetry factor α [51].

The standard reaction rate constant k_0 was estimated for each investigated electrode process using peak potential separation ΔE, through approximation coefficient Y [50]. The rate constant can be obtained from Y by means of Eq. (2). Following approach is well suited for quasi-reversible and nonreversible processes.

$$Y = \left(\frac{D_{ox}}{D_{red}}\right)^{\alpha/2} * k_0 \frac{\sqrt{RT}}{\sqrt{nFvD_{ox}}} \quad (2)$$

where: R, T, n, F have their usual meaning, D_{ox} and D_{red} are diffusion coefficient of ferri- and ferrocyanides and equal to 0.738×10^{-6} cm^2/s and 0.726×10^{-6} cm^2/s, respectively [59], $\alpha = 0.5$ is symmetry factor and *v* is scan rate in *V*/s.

The results are summarized in Table 3. It is clearly visible that the 20 k electrode possesses one order of magnitude higher values of standard rate constant, allowing them to achieve equilibrium state much faster and supporting previous evidence overall lower electrochemical activity of the 10 k electrodes' reaction plane. Higher peak currents are promoted on the top surface of investigated nanosheet electrodes, suggesting lower charge

transfer resistance of $Fe(CN)_6^{3-/4-}$ oxidation/reduction or larger reaction plane.

An increase in sweeping rate promotes growth of current peak intensity in both cathodic and anodic reactions and revealing a linear dependence with the square root of the scan rate passing through zero. This can be seen in the inset of Fig. 4. The relationship $i_p = f(v^{1/2})$ for quasi-reversible electrodes was described by Nicholson and Shain as a derivative of the Randles-Sevcik reversible theory [60]. The estimated electrochemical active surface appears to be always higher on the top surface rather than bottom side of the electrode. This phenomenon indicates that increasing boron doping density leads to formation of different crystal structure, which influences significant changes in the electron transfer process.

4. Conclusions

We have proposed a novel approach to obtain thin BDD foils, grown on Ta substrate and easily transferred to PDMS substrate. The [B]/[C] ratio of 10 k and 20 k ppm, characteristic for heavy boron-doped diamond films was confirmed using Raman spectroscopy. SEM micrographs reveal structural differences between top surface and bottom side of the BDD foil, regardless of the studied boron concentration. The bottom side was flat as a result of direct contact with tantalum, characterized by more deformed structure and smaller grain size, as expected. The differentiation between top and bottom side of the foil translates to modified physic-chemical and electrochemical behavior of studied electrodes.

The electrochemical activity significantly depends on boron incorporation, increasing with increased boron dopant density. The highest level of reversibility of the electrochemical process and the highest value of equilibrium constant k_0 was recorded at the top surface of 20 k ppm [B]/[C] BDD foil. At the same time, the kinetics of the Faradaic process is hindered at the bottom side of the electrodes. The bottom sides of the foils are characterized with lower reaction rate constants supporting their partial blockade. Results of voltammetry studies confirmed that overlapping of factors arising from surface functionalities, boron doping level, crystallite size and grain boundaries affect the electron transfer kinetics on surface of BDD foil. This significant observation highlights the importance of nanoscale size structure in functionality of boron-doped diamond nanosheets.

Author contribution section

Robert Bogdanowicz: Conceptualization, Methodology, Supervision, Writing- Original draft preparation, Writing- Reviewing and Editing, Funding acquisition.

Mateusz Ficek: Conceptualization, Investigation, Writing- Original draft preparation.

Natalia Malinowska: Investigation, Data Curation, Visualization.

Sanju Gupta: Conceptualization, Methodology.

Romney Meek: Investigation, Data Curation.

Paweł Niedziałkowski: Investigation, Data Curation, Visualization, Writing- Original draft preparation, Writing- Reviewing and Editing.

Michał Rycewicz: Investigation, Data Curation, Visualization, Writing-Original draft preparation.

Mirosław Sawczak: Investigation, Data Curation, Visualization, Writing-Original draft preparation,

Jacek Ryl: Conceptualization, Methodology, Writing- Original draft preparation, Writing- Reviewing and Editing.

Tadeusz Ossowski: Validation, Writing- Reviewing and Editing, Funding acquisition.

Declaration of competing interest

The authors declare that they have no known competing financial interests or personal relationships that could have appeared to influence the work reported in this paper.

Acknowledgments

The authors gratefully acknowledge financial support in parts from the National Science Centre (NCN) under Grant No. 2016/21/B/ST7/01430, 2016/22/E/ST7/00102, 2015/17/D/ST5/02571 and the National Centre for Research and Development Grant Techmatstrateg No. 347324. This work was partially supported by the Science for Peace Programme of NATO (Grant no. G5147). The DS funds of the Faculty of Electronics, Telecommunications and Informatics of the Gdańsk University of Technology are also acknowledged. The author (S.G.) acknowledges KSEF-RDE (Grant #148-502-17-397), KY NSF EPSCoR RSP (subaward #3200000271-17-212), KY NSF EPSCoR REG (subaward #3200000271-18-059), and KY NASA EPSCoR (RID-3-NNX15AK28A, subaward #3200000029-17-229) grants and Bryce Aberg (graduate student) for developing Matlab script.

Appendix A. Supplementary data

Supplementary data to this article can be found online at https://doi.org/10.1016/j.jelechem.2020.114016.

References

[1] C.J.H. Wort, R.S. Balmer, Diamond as an electronic material, Mater. Today 11 (2008) 22–28, https://doi.org/10.1016/S1369-7021(07)70349-8.
[2] N. Yang, J.S. Foord, X. Jiang, Diamond electrochemistry at the nanoscale: a review, Carbon 99 (2016) 90–110, https://doi.org/10.1016/j.carbon.2015.11.061.
[3] P.B. Shah, J. Weil, A.G. Birdwell, T. Ivanov, Charge trapping analysis of high speed diamond FETs, MRS Adv 2 (2017) 2235–2240, https://doi.org/10.1557/adv.2017.141.
[4] D. Nidzworski, K. Siuzdak, P. Niedziałkowski, R. Bogdanowicz, M. Sobaszek, J. Ryl, P. Weiher, M. Sawczak, E. Wnuk, W.A. Goddard, A. Jaramillo-Botero, T. Ossowski, A rapid-response ultrasensitive biosensor for influenza virus detection using antibody modified boron-doped diamond, Sci. Rep. 7 (2017) 15707, https://doi.org/10.1038/s41598-017-15806-7.
[5] A. Bellucci, P. Calvani, M. Girolami, S. Orlando, R. Polini, D.M. Trucchi, Optimization of black diamond films for solar energy conversion, Appl. Surf. Sci. 380 (2016) 8–11, https://doi.org/10.1016/j.apsusc.2016.02.107.
[6] S. Yu, N. Yang, H. Zhuang, S. Mandal, O.A. Williams, B. Yang, N. Huang, X. Jiang, Battery-like supercapacitors from diamond networks and water-soluble redox electrolytes, J. Mater. Chem. A 5 (2017) 1778–1785, https://doi.org/10.1039/C6TA08607A.
[7] C.E. Nebel, N. Yang, H. Uetsuka, E. Osawa, N. Tokuda, O. Williams, Diamond nanowires, a new approach towards next generation electrochemical gene sensor platforms, Diam. Relat. Mater. 18 (2009) 910–917, https://doi.org/10.1016/j.diamond.2008.11.024.
[8] T.A. Enache, A.M. Oliveira-Brett, Boron doped diamond and glassy carbon electrodes comparative study of the oxidation behaviour of cysteine and methionine, Bioelectrochemistry 81 (2011) 46–52, https://doi.org/10.1016/j.bioelechem.2011.02.001.
[9] H. Yu, H. Wang, X. Quan, S. Chen, Y. Zhang, Amperometric determination of chemical oxygen demand using boron-doped diamond (BDD) sensor, Electrochem. Commun. 9 (2007) 2280–2285, https://doi.org/10.1016/j.elecom.2007.06.037.
[10] T.A. Ivandini, B.V. Sarada, C. Terashima, T.N. Rao, D.A. Tryk, H. Ishiguro, Y. Kubota, A. Fujishima, Electrochemical detection of tricyclic antidepressant drugs by HPLC using highly boron-doped diamond electrodes, J. Electroanal. Chem. 521 (2002) 117–126, https://doi.org/10.1016/S0022-0728(02)00666-6.
[11] C. Prado, S.J. Wilkins, F. Marken, R.G. Compton, Simultaneous electrochemical detection and determination of lead and copper at boron-doped diamond film electrodes, Electroanalysis 14 (2002) 262–272, https://doi.org/10.1002/1521-4109(200202)14:4<262::AID-ELAN262>3.0.CO;2-D.
[12] Y. Yu, Y. Zhou, L. Wu, J. Zhi, Electrochemical biosensor based on boron-doped diamond electrodes with modified surfaces, Int. J. Electrochem. (2012), 567171. https://doi.org/10.1155/2012/567171.
[13] Y.L. Zhou, R.H. Tian, J.F. Zhi, Amperometric biosensor based on tyrosinase immobilized on a boron-doped diamond electrode, Biosens. Bioelectron. 22 (2007) 822–828, https://doi.org/10.1016/j.bios.2006.03.001.
[14] C. Comninellis, Electrocatalysis in the electrochemical conversion/combustion of organic pollutants for waste water treatment, Electrochim. Acta 39 (1994) 1857–1862, https://doi.org/10.1016/0013-4686(94)85175-1.
[15] K. Honda, M. Yoshimura, T.N. Rao, D.A. Tryk, A. Fujishima, K. Yasui, Y. Sakamoto, K. Nishio, H. Masuda, Electrochemical properties of Pt-modified nano-honeycomb diamond electrodes, J. Electroanal. Chem. 514 (2001) 35–50, https://doi.org/10.1016/S0022-0728(01)00614-3.
[16] E. Guinea, F. Centellas, E. Brillas, P. Cañizares, C. Sáez, M.A. Rodrigo, Electrocatalytic properties of diamond in the oxidation of a persistant pollutant, Appl. Catal. B Environ. 89 (2009) 645–650, https://doi.org/10.1016/j.apcatb.2009.01.028.
[17] H.B. Martin, A. Argoitia, U. Landau, A.B. Anderson, J.C. Angus, Hydrogen and oxygen evolution on boron-doped diamond electrodes, J. Electrochem. Soc. 143 (1996) L133–L136, https://doi.org/10.1149/1.1836901.
[18] R. Bogdanowicz, J. Czupryniak, M. Gnyba, J. Ryl, T. Ossowski, M. Sobaszek, E.M. Siedlecka, K. Darowicki, Amperometric sensing of chemical oxygen demand at glassy

carbon and silicon electrodes modified with boron-doped diamond, Sens. Actuators B Chem. 189 (2013) 30–36, https://doi.org/10.1016/j.snb.2012.12.007.
[19] B.P. Chaplin, I. Wyle, H. Zeng, J.A. Carlisle, J. Farrell, Characterization of the performance and failure mechanisms of boron-doped ultrananocrystalline diamond electrodes, J. Appl. Electrochem. 41 (2011) 1329–1340, https://doi.org/10.1007/s10800-011-0351-7.
[20] G.M. Swain, The susceptibility to surface corrosion in acidic fluoride media: a comparison of diamond, HOPG, and glassy carbon electrodes, J. Electrochem. Soc. 141 (1994) 3382–3393, https://doi.org/10.1149/1.2059343.
[21] A. Fujishima, Diamond Electrochemistry, BKC ; Elsevier, Tokyo; Amsterdam; Boston, 2005.
[22] A. Suzuki, T.A. Ivandini, K. Yoshimi, A. Fujishima, G. Oyama, T. Nakazato, N. Hattori, S. Kitazawa, Y. Einaga, Fabrication, characterization, and application of boron-doped diamond microelectrodes for in vivo dopamine detection, Anal. Chem. 79 (2007) 8608–8615, https://doi.org/10.1021/ac071519h.
[23] K. Pecková, J. Musilová, J. Barek, Boron-doped diamond film electrodes—new tool for voltammetric determination of organic substances, Crit. Rev. Anal. Chem. 39 (2009) 148–172, https://doi.org/10.1080/10408340903011812.
[24] R. Bogdanowicz, M. Śmietana, M. Gnyba, M. Ficek, V. Straňák, Ł. Goluński, M. Sobaszek, J. Ryl, Nucleation and growth of CVD diamond on fused silica optical fibres with titanium dioxide interlayer, Phys. Status Solidi A. 210 (2013) 1991–1997, https://doi.org/10.1002/pssa.201300096.
[25] M. Smietana, J. Szmidt, M.L. Korwin-Pawlowski, W.J. Bock, J. Grabarczyk, Application of diamond-like carbon films in optical fibre sensors based on long-period gratings, Diam. Relat. Mater. 16 (2007) 1374–1377, https://doi.org/10.1016/j.diamond.2006.11.018.
[26] A. Aleksov, M. Kubovic, N. Kaeb, U. Spitzberg, A. Bergmaier, G. Dollinger, Th. Bauer, M. Schreck, B. Stritzker, E. Kohn, Diamond field effect transistors—concepts and challenges, Diam. Relat. Mater. 12 (2003) 391–398, https://doi.org/10.1016/S0925-9635(02)00401-6.
[27] V.A. Kukushkin, S.A. Bogdanov, Simulation of CVD diamond-based high speed near-infrared photodetectors, Diam. Relat. Mater. 60 (2015) 94–98, https://doi.org/10.1016/j.diamond.2015.10.017.
[28] V. Seshan, J.O. Island, R. van Leeuwen, W.J. Venstra, B.H. Schneider, S.D. Janssens, K. Haenen, E.J.R. Sudhölter, L.C.P.M. de Smet, H.S.J. van der Zant, G.A. Steele, A. Castellanos-Gomez, Pick-up and drop transfer of diamond nanosheets, Nanotechnology 26 (2015) 125706, https://doi.org/10.1088/0957-4484/26/12/125706.
[29] M.A. Lodes, S.M. Rosiwal, R.F. Singer, Self-supporting nanocrystalline diamond foils – a new concept for crystalline diamond on any technical surface, Key Eng. Mater. 438 (2010) 163–169, https://doi.org/10.4028/www.scientific.net/KEM.438.163.
[30] J. Fecher, M. Wormser, S.M. Rosiwal, Long term oxidation behavior of micro- and nanocrystalline CVD diamond foils, Diam. Relat. Mater. 61 (2016) 41–45, https://doi.org/10.1016/j.diamond.2015.11.009.
[31] Y. Yardım, M. Gülcan, Z. Şentürk, Determination of vanillin in commercial food product by adsorptive stripping voltammetry using a boron-doped diamond electrode, Food Chem. 141 (2013) 1821–1827, https://doi.org/10.1016/j.foodchem.2013.04.085.
[32] C. Radovan, C. Cofan, D. Cinghita, Simultaneous determination of acetaminophen and ascorbic acid at an unmodified boron-doped diamond electrode by differential pulse voltammetry in buffered media, Electroanalysis 20 (2008) 1346–1353, https://doi.org/10.1002/elan.200804188.
[33] N. Yang, J.S. Foord, X. Jiang, Diamond electrochemistry at the nanoscale: a review, Carbon 99 (2016) 90–110, https://doi.org/10.1016/j.carbon.2015.11.061.
[34] S.J. Cobb, Z.J. Ayres, J.V. Macpherson, Boron doped diamond: a designer electrode material for the twenty-first century, Annu. Rev. Anal. Chem. 11 (2018) 463–484, https://doi.org/10.1146/annurev-anchem-061417-010107.
[35] K. Siuzdak, R. Bogdanowicz, Nano-engineered diamond-based materials for Supercapacitor electrodes: a review, Energy Technol 6 (2018) 223–237, https://doi.org/10.1002/ente.201700345.
[36] S. Baluchová, A. Daňhel, H. Dejmková, V. Ostatná, M. Fojta, K. Schwarzová-Pecková, Recent progress in the applications of boron doped diamond electrodes in electroanalysis of organic compounds and biomolecules – a review, Anal. Chim. Acta 1077 (2019) 30–66, https://doi.org/10.1016/j.aca.2019.05.041.
[37] C.P. Sousa, F.W.P. Ribeiro, T.M.B.F. Oliveira, G.R. Salazar-Banda, P. de Lima-Neto, S. Morais, A.N. Correia, Electroanalysis of pharmaceuticals on boron-doped diamond electrodes: a review, ChemElectroChem 6 (2019) 2350–2378, https://doi.org/10.1002/celc.201801742.
[38] M. Diaz, M. Cataldo, P. Ledezma, J. Keller, K. Doederer, Unravelling the mechanisms controlling the electro-generation of ferrate using four iron salts in boron-doped diamond electrodes, J. Electroanal. Chem. 854 (2019), 113501. https://doi.org/10.1016/j.jelechem.2019.113501.
[39] T.A. Ivandini, T. Watanabe, T. Matsui, Y. Ootani, S. Iizuka, R. Toyoshima, H. Kodama, H. Kondoh, Y. Tateyama, Y. Einaga, Influence of surface orientation on electrochemical properties of boron-doped diamond, J. Phys. Chem. C 123 (2019) 5336–5344, https://doi.org/10.1021/acs.jpcc.8b10406.
[40] M. Ficek, M. Sobaszek, M. Gnyba, J. Ryl, Ł. Gołuński, M. Smietana, J. Jasiński, P. Caban, R. Bogdanowicz, Optical and electrical properties of boron doped diamond thin conductive films deposited on fused silica glass substrates, Appl. Surf. Sci. 387 (2016) 846–856, https://doi.org/10.1016/j.apsusc.2016.06.165.
[41] R. Bogdanowicz, M. Sobaszek, M. Ficek, M. Gnyba, J. Ryl, K. Siuzdak, W.J. Bock, M. Smietana, Opto-electrochemical sensing device based on long-period grating coated with boron-doped diamond thin film, J Opt Soc Korea 19 (2015) 705–710.
[42] M. Tsigkourakos, T. Hantschel, D.K. Simon, T. Nuytten, A.S. Verhulst, B. Douhard, W. Vandervorst, On the local conductivity of individual diamond seeds and their impact on the interfacial resistance of boron-doped diamond films, Carbon 79 (2014) 103–112, https://doi.org/10.1016/j.carbon.2014.07.048.
[43] R. Bogdanowicz, M. Ficek, M. Sobaszek, A. Nosek, Ł. Gołuński, J. Karczewski, A. Jaramillo-Botero, W.A. Goddard, M. Bockrath, T. Ossowski, Growth and isolation of large area boron-doped nanocrystalline diamond sheets: a route toward diamond-on-graphene heterojunction, Adv. Funct. Mater. 29 (2019) 1805242, https://doi.org/10.1002/adfm.201805242.
[44] J. Schindelin, I. Arganda-Carreras, E. Frise, V. Kaynig, M. Longair, T. Pietzsch, S. Preibisch, C. Rueden, S. Saalfeld, B. Schmid, J.-Y. Tinevez, D.J. White, V. Hartenstein, K. Eliceiri, P. Tomancak, A. Cardona, Fiji: an open-source platform for biological-image analysis, Nat. Methods 9 (2012) 676–682, https://doi.org/10.1038/nmeth.2019.
[45] S. Gupta, B. McDonald, S.B. Carrizosa, Surface redox chemistry of immobilized nanodiamond: effects of particle size and electrochemical environment, J. Electron. Mater. 46 (2017) 4512–4526, https://doi.org/10.1007/s11664-017-5426-8.
[46] S. Gupta, B. Evans, A. Henson, S.B. Carrizosa, S. Gupta, B. Evans, A. Henson, S.B. Carrizosa, Salt-assisted ultrasonicated de-aggregation and advanced redox electrochemistry of detonation nanodiamond, Materials 10 (2017) 1292, https://doi.org/10.3390/ma10111292.
[47] V. Mortet, Z. Vlčková Živcová, A. Taylor, O. Frank, P. Hubík, D. Trémouilles, F. Jomard, J. Barjon, L. Kavan, Insight into boron-doped diamond Raman spectra characteristic features, Carbon 115 (2017) 279–284, https://doi.org/10.1016/j.carbon.2017.01.022.
[48] S.W. da Silva, E.M.O. Navarro, M.A.S. Rodrigues, A.M. Bernardes, V. Pérez-Herranz, The role of the anode material and water matrix in the electrochemical oxidation of norfloxacin, Chemosphere 210 (2018) 615–623, https://doi.org/10.1016/j.chemosphere.2018.07.057.
[49] M. Śmietana, P. Niedziałkowski, W. Białobrzeska, D. Burnat, P. Sezemsky, M. Koba, V. Stranak, K. Siuzdak, T. Ossowski, R. Bogdanowicz, Study on combined optical and electrochemical analysis using indium-tin-oxide-coated optical fiber sensor, Electroanalysis 31 (2019) 398–404, https://doi.org/10.1002/elan.201800638.
[50] R. Holze, Experimental Electrochemistry: A Laboratory Textbook, WILEY-VCH Verlag GmbH & Co. KGaA, Weinheim, 2009.
[51] B. Allen, F. Larry, Electrochemical Methods: Fundamentals and Applications, 2nd ed. John Wiley & Sons, Inc, United States of America, 2001.
[52] R. Bogdanowicz, A. Fabiańska, L. Golunski, M. Sobaszek, M. Gnyba, J. Ryl, K. Darowicki, T. Ossowski, S.D. Janssens, K. Haenen, E.M. Siedlecka, Influence of the boron doping level on the electrochemical oxidation of the azo dyes at Si/BDD thin film electrodes, Diam. Relat. Mater. 39 (2013) 82–88, https://doi.org/10.1016/j.diamond.2013.08.004.
[53] A. Zieliński, R. Bogdanowicz, J. Ryl, L. Burczyk, K. Darowicki, Local impedance imaging of boron-doped polycrystalline diamond thin films, Appl. Phys. Lett. 105 (2014), 131908. https://doi.org/10.1063/1.4897346.
[54] Y. Pleskov, Y. Evstefeeva, M.D. Krotova, V.P. Varnin, I.G. Teremetskaya, Synthetic semiconductor diamond electrodes: electrochemical behaviour of homoepitaxial boron-doped films orientated as (111), (110), and (100) faces, J. Electroanal. Chem. 595 (2006) 168–174, https://doi.org/10.1016/j.jelechem.2006.07.010.
[55] H. Girard, N. Simon, D. Ballutaud, M. Herlem, A. Etcheberry, Effect of anodic and cathodic treatments on the charge transfer of boron doped diamond electrodes, Diam. Relat. Mater. 16 (2007) 316–325, https://doi.org/10.1016/j.diamond.2006.06.009.
[56] J. Ryl, L. Burczyk, R. Bogdanowicz, M. Sobaszek, K. Darowicki, Study on surface termination of boron-doped diamond electrodes under anodic polarization in H2SO4 by means of dynamic impedance technique, Carbon 96 (2016) 1093–1105, https://doi.org/10.1016/j.carbon.2015.10.064.
[57] T.J. Davies, C.E. Banks, R.G. Compton, Voltammetry at spatially heterogeneous electrodes, J. Solid State Electrochem. 9 (2005) 797–808, https://doi.org/10.1007/s10008-005-0699-x.
[58] T.J. Davies, R.R. Moore, C.E. Banks, R.G. Compton, The cyclic voltammetric response of electrochemically heterogeneous surfaces, J. Electroanal. Chem. 574 (2004) 123–152, https://doi.org/10.1016/j.jelechem.2004.07.031.
[59] S.J. Konopka, Bruce. McDuffie, Diffusion coefficients of ferri- and ferrocyanide ions in aqueous media, using twin-electrode thin-layer electrochemistry, Anal. Chem. 42 (1970) 1741–1746, https://doi.org/10.1021/ac50160a042.
[60] R.S. Nicholson, I. Shain, Theory of stationary electrode polarography. Single scan and cyclic methods applied to reversible, irreversible, and kinetic systems, Anal. Chem. 36 (1964) 706–723, https://doi.org/10.1021/ac60210a007.